

CHAPTER 3

RESULTS AND DISCUSSION

3.1 CHAPTER OUTLINE

This chapter presents the data obtained from the investigation of each of the following possible explanations:

- (1) Experimental artifacts.
- (2) Direct energy transfer to luminescence traps.
- (3) Two-photon absorption, excited-state absorption, and second harmonic generation (SHG).
- (4) Superfluorescence and amplified spontaneous emission.
- (5) Localized heating.
- (6) Up-conversion by energy transfer.

Each phenomenon will be explained in detail along with a justification of why it was considered. The results demonstrate that explanations (1) → (5) must be ruled out and all evidence supports (6), the mechanism of up-conversion by energy transfer.

3.2 EXPERIMENTAL ARTIFACTS

Before considering possible nonlinear explanations we must rule out experimental artifacts. The first to be considered was detector saturation. A detector is saturated when it is no longer able to produce an electrical output proportional to the magnitude of incident radiation. The most likely point for detector saturation in an excitation spectrum would be at emission maxima, and might be recorded as a dip in the spectra. That possibility was ruled out by placing neutral density filters between the sample and the monochromator to decrease the amount incident radiation reaching the detector. This ensured that the magnitude of incident radiation was not large enough to cause saturation. The resulting excitation spectra showed a uniform signal decrease, however the dips in the excitation spectra remained.

Other possible experimental limitations considered were incomplete signal integration and the detector time response being too slow. Both of these limitations were ruled out because the dip corresponds to a decrease in luminescence signal occurring several microseconds after excitation.

3.3 DIRECT TRANSFER TO TRAPS

As discussed in the background section, energy transfer to traps can occur in Eu_2O_3 because of the high concentration of Eu^{3+} ions. This trapping is referred to as concentration quenching and results in an overall decrease in luminescence output. If direct transfer to traps causes the dips, the phenomena

should show no dependence on excitation density.^[1] However, an excitation energy dependence study showed that the excitation dip was density dependent (refer to Figure 6). At low excitation density the dip was not present. It only appeared at excitation energies above 70-mJ. Thus the dip shows a direct dependence on excitation density and cannot be attributed to energy transfer to traps.

3.4 MULTIPLE PHOTON ABSORPTION

With experimental artifacts and energy transfer to traps ruled out, the dips in the excitation spectra could only be explained in terms of a nonlinear relationship between excitation density and luminescence output. The first nonlinear process investigated was the multiple absorption of photons by individual Eu^{3+} ions. This process has been reported to occur in a number of luminescent systems including those doped with rare earth ions.^[2] The three possible mechanisms for multiple-photon absorption are illustrated using simplified energy diagrams (refer to Figure 7). It is important to note that all three processes require a high excitation density and only occur during the laser excitation pulse.

The process of 2-photon absorption occurs when an ion absorbs two photons simultaneously, each at half the resonance frequency of an excited state. Second harmonic generation (SHG) occurs when two photons are

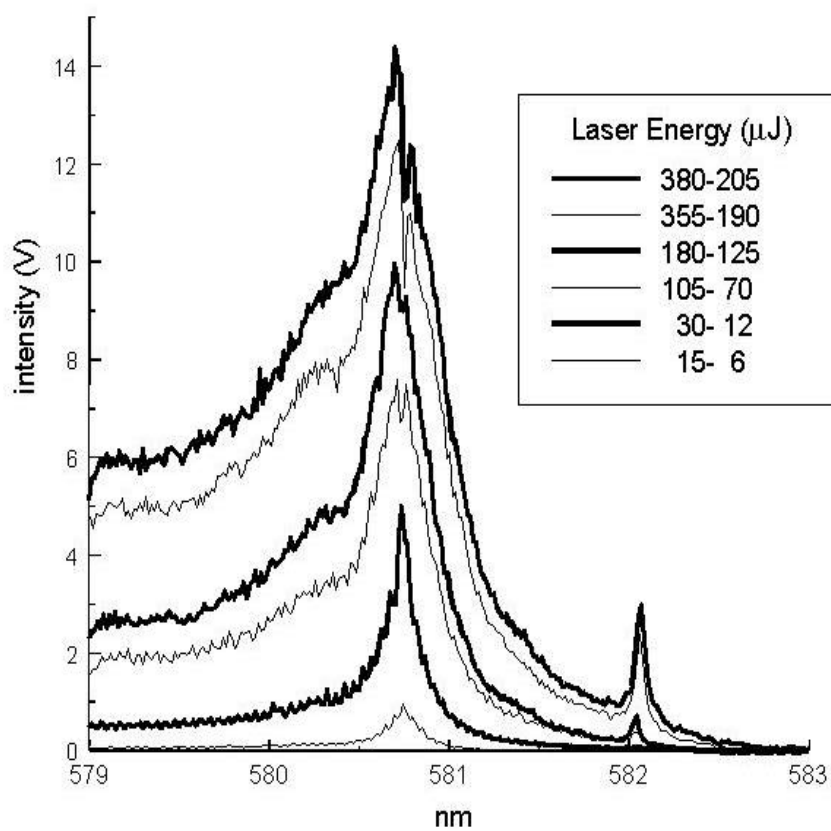


Figure 6. Excitation spectra of Eu₂O₃ (cubic-phase, micron-sized crystals) Sample temperature 11K

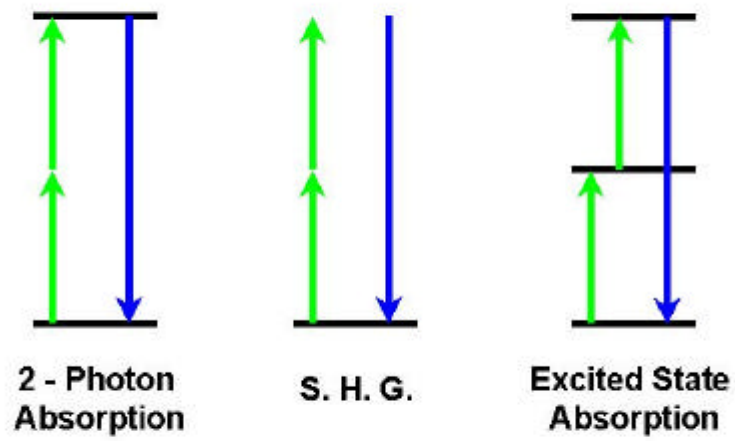
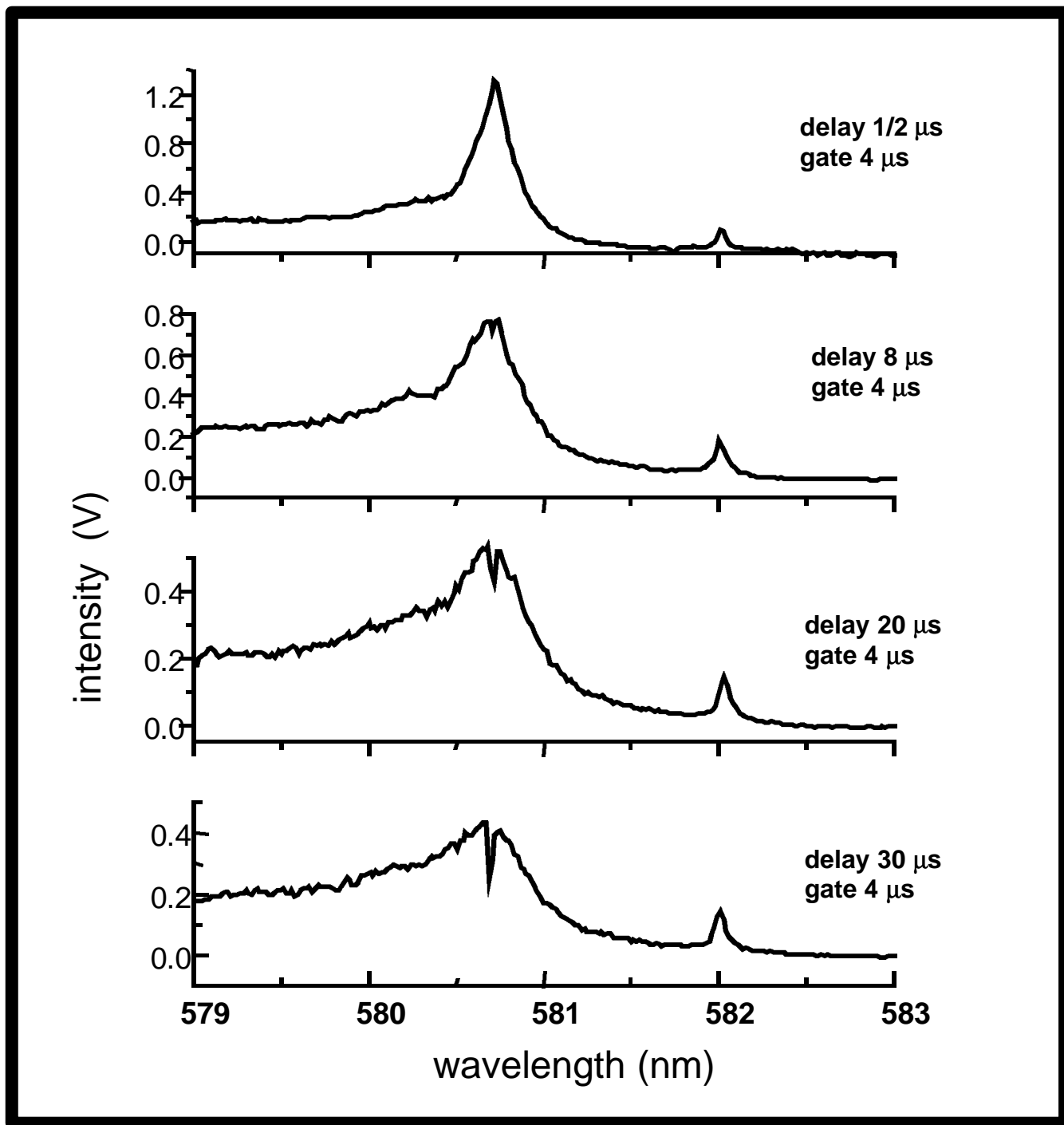


Figure 7. Energy schemes for the different 2-photon absorption processes

absorbed simultaneously, each at half the resonance frequency of a virtual excited level. The third process, Excited-state absorption, also involves absorption of two photons by a single ion. In this case, however, the first absorbed photon promotes the ion to an excited-state level with a finite lifetime and not to a virtual level with a lifetime of zero. Since the ion can remain excited during the entire laser pulse it has a much higher probability of absorbing a second photon, compared to 2-photon absorption and SHG which require that both photons be absorbed simultaneously.^[3]

Each of the multiple photon processes can potentially result in emission of a high-energy anti-Stokes luminescence. Emission at a higher energy was not emitted from the Eu_2O_3 system. The lack of anti-Stokes luminescence alone cannot be used to rule out multiple photon absorption, because excitation to high-energy states would be quickly followed by nonradiative decay to the lower-energy $^5\text{D}_0$ excited state.^[4, 5]

Multiple photon absorption was investigated by collecting excitation spectra of Eu_2O_3 using various delay times. The resulting spectra are presented (refer to Figure 8). The first excitation spectrum was collected utilizing a delay of $\frac{1}{2}$ -ms and a gate of 4-ms. These experimental parameters selectively integrated the luminescence occurring immediately after excitation, and the spectrum showed no dip at the absorption maxima. The additional spectra presented in Figure 3 were collected using the longer delay times of 8, 20, and 30-ms respectively. The spectra collected after a delay of 8 ms shows a small dip at the absorption maxima. This dip increases upon going to longer 20 and 30-ms



**Figure 8. Excitation spectra for Eu_2O_3 using various delay times (cubic-phase, micron-sized crystals)
Sample temperature 11K**

delays. This data clearly demonstrates that the phenomenon causing the saturation dip occurs after the exciting laser pulse has ceased. This rules out all three multiple-photon processes as possible explanations for the saturation dips since each must occur during the excitation pulse.

3.5 AMPLIFIED SPONTANEOUS EMISSION

Other nonlinear effects considered included superfluorescence, amplified spontaneous emission, and stimulated emission. Each of these processes are known to occur in rare earth systems, and are of particular interest in the field of laser science. Each process would require a high density of excited states that would only be possible at absorption maxima, and any one of these processes could potentially explain the saturation dip. The mechanisms for the first two processes are presented in Figure 9.

Superfluorescence occurs when a large population of atoms prepared initially in a state of complete inversion undergoes relaxation by collective

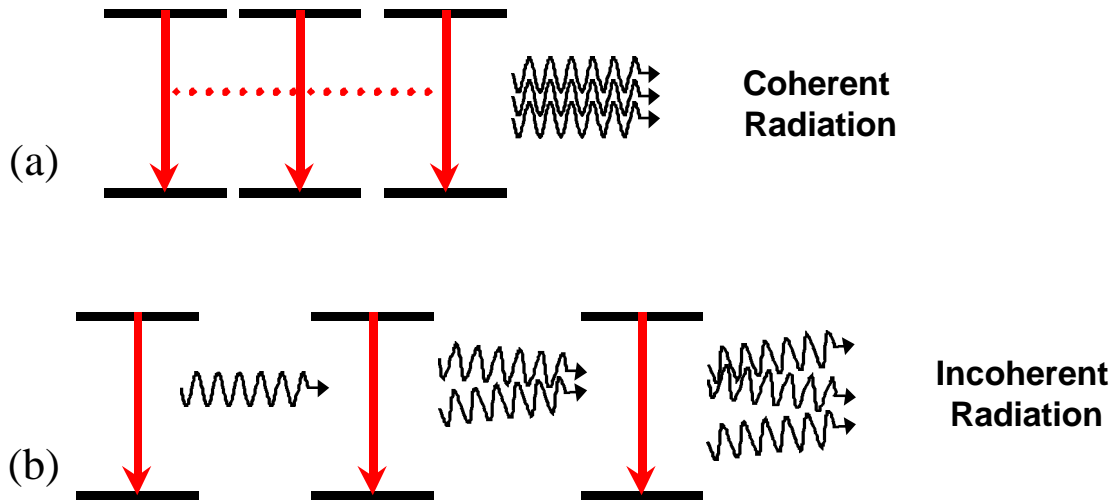


Figure 9. (a) Superfluorescence
(b) Amplified spontaneous emission

spontaneous decay.^[6] The collection of excited ions act as one large dipole and simultaneously emit coherent radiation. In order for superfluorescence to be possible the excited ions must be in close proximity and they must be excited coherently. This process is known to compete with stimulated emission in certain rare earth laser materials.^[7]

Amplified spontaneous emission occurs when spontaneous emission from a single atom is amplified as it propagates. This process differs from amplified stimulated emission because the propagating photon triggers other excited ions to emit; it does not stimulate emission. Unlike stimulated emission, all emitted photons do not travel in the same direction. Thus the resulting emission is incoherent.^[6]

Line narrowing is usually quite profound for examples of superfluorescence and amplified spontaneous emission. For example the emission spectrum of NdCl_3 shows about 20 sharp lines in the range of 550 to 700 nm when excitation power is below 230 mW.^[7] However superfluorescence occurs when the excitation power is above the 230-mW threshold. The emission spectra peaks only at 694.4 nm and this peak clearly shows a spectral narrowing effect.^[7]

From an examination of the fluorescence emission from Eu_2O_3 it is possible to determine whether superfluorescence, amplified spontaneous emission, or stimulated emission is responsible for the saturation dip. In each case some degree of fluorescent line narrowing along with shortening of fluorescent lifetime should be expected. Fluorescence spectra were obtained for

Eu_2O_3 at various excitation densities (refer to Figure 10). The portion of Eu_2O_3 fluorescence spectrum presented corresponds to $^5\text{D}_0 \rightarrow ^7\text{F}_2$ transitions in the 605 to 630-nm range. Of the luminescent transitions possible for Eu_2O_3 , $^5\text{D}_0 \rightarrow ^7\text{F}_2$ has the highest transition probability with the largest peak occurring at ~612 nm. Two smaller peaks are also present at ~614 nm and ~630 nm. For each of the overlaid spectra the peak-to-peak ratio is independent of excitation density. If either superfluorescence, amplified spontaneous emission, or stimulated emission were occurring, the peak at 612 nm should dominate the emission spectrum or at the very least increase in size relative to the other emission lines. The fact that this does not occur and that fluorescent line narrowing is also absent rules out these nonlinear processes as possible explanations.

3.6 LOCALIZED HEATING

As presented in the background section, concentration quenching is known to occur in Eu_2O_3 and as a result ~97% of absorbed radiation is quenched at luminescence traps. Once the energy of an excited Eu^{3+} ion is transferred to a trap, nonradiative decay converts the energy to heat. Since energy transfer in Eu_2O_3 is phonon assisted, an accumulation of heat might increase the rate of energy transfer to traps, shortening the fluorescence lifetime. The effects of localized heating were investigated because the largest amounts of heat would be produced at absorption maxima, which could lead to the observed saturation dips.

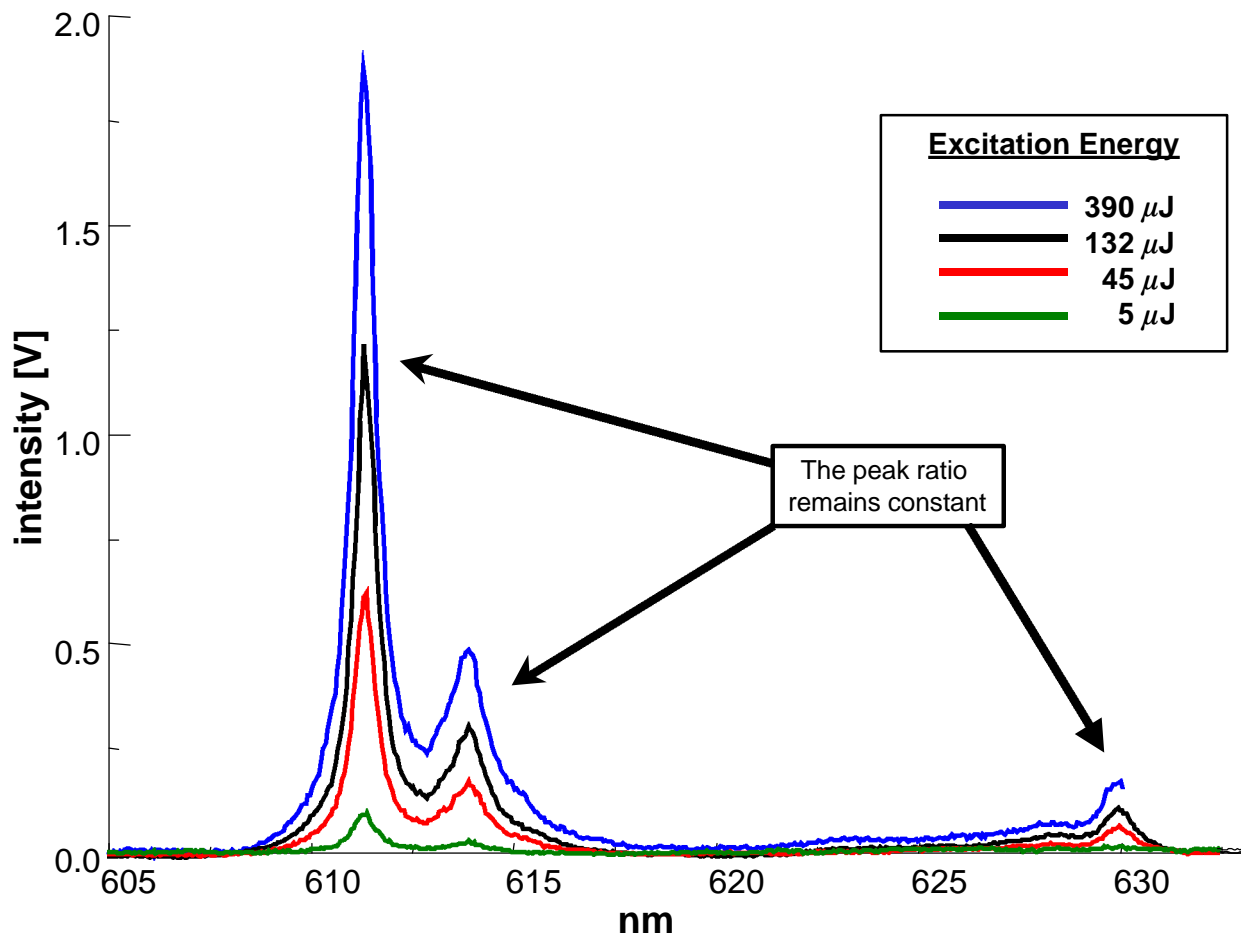


Figure 10. ${}^5\text{D}_0 \rightarrow {}^7\text{F}_2$ Fluorescence of Eu_2O_3 at various excitation densities. (cubic-phase, micron-sized crystals) Temp 11K

The influence that temperature has on fluorescence decay in Eu_2O_3 is presented as a plot of lifetime vs. temperature (refer to Figure 11). The plot shows that as temperature is increased from 11K to 90K, the fluorescence lifetime decreases. Above 90K, temperature has little influence on fluorescence decay. This behavior has been confirmed by a study on energy transfer in Eu_2O_3 by M. Buijs in which it was determined that fluorescence lifetime does not change above 90K.^[8]

If localized heating was shortening the fluorescence lifetime at the absorption maxima, that might explain the dip in the excitation spectra. A temperature dependency study on the excitation spectra tended to disprove this theory (refer to Figure 12). Several spectra excited at high excitation density were taken at various temperatures. The saturation dip is visible in the excitation spectra up to temperatures of 200K. If the dip was a result of localized heating shortening fluorescence lifetimes, then it should not be present at temperatures above 90K.

There are also additional arguments against localized heating. First of all the saturation dip can be produced using an excitation pulse of less than 30 mJ, and this amount of energy seems too small to be responsible for a large temperature increase. Secondly, all experiments utilized pulsed excitation and accumulation of heat should be minimal. This was confirmed by examining the excitation of “hot bands” (refer to Figure 13). At 11K almost all of the Eu^{3+} ions will be in the ${}^7\text{F}_0$ ground state, however excitation spectra show small peaks at 582 nm which correspond to the ${}^7\text{F}_1 \rightarrow {}^5\text{D}_0$ transition. Transitions out of the ${}^7\text{F}_1$

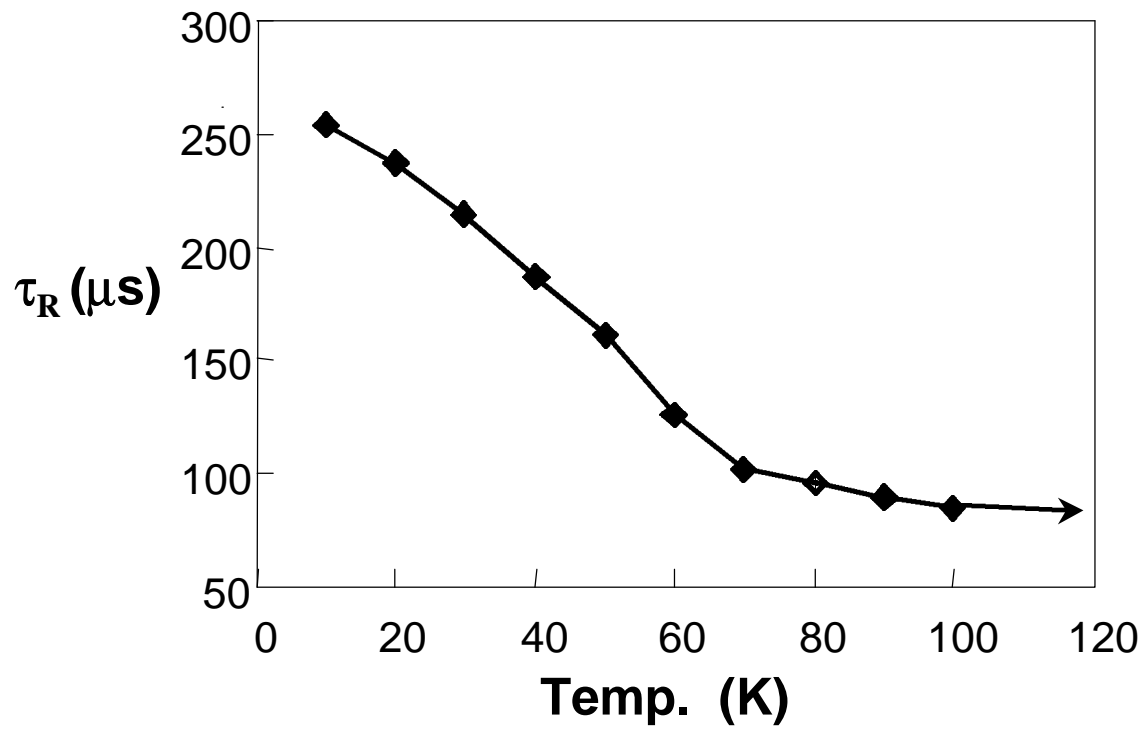
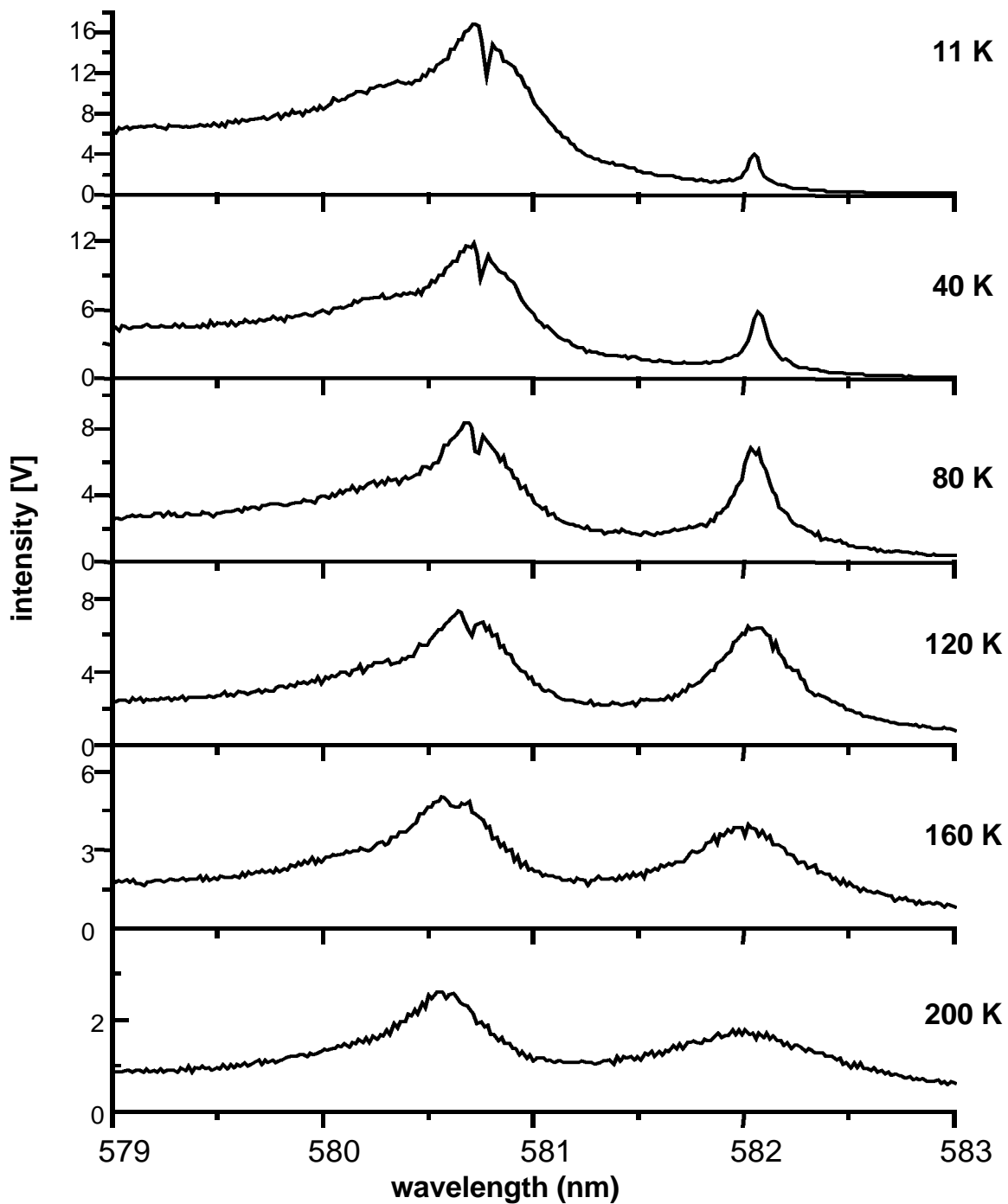


Figure 11. Plot of fluorescence decay vs. temperature.
Estimated as a single exponential decay
{ $I = I_0 \exp(-t/\tau_R)$ }



**Figure 12. Eu_2O_3 excitation spectra vs. temperature.
(cubic-phase, micron-sized crystals)**

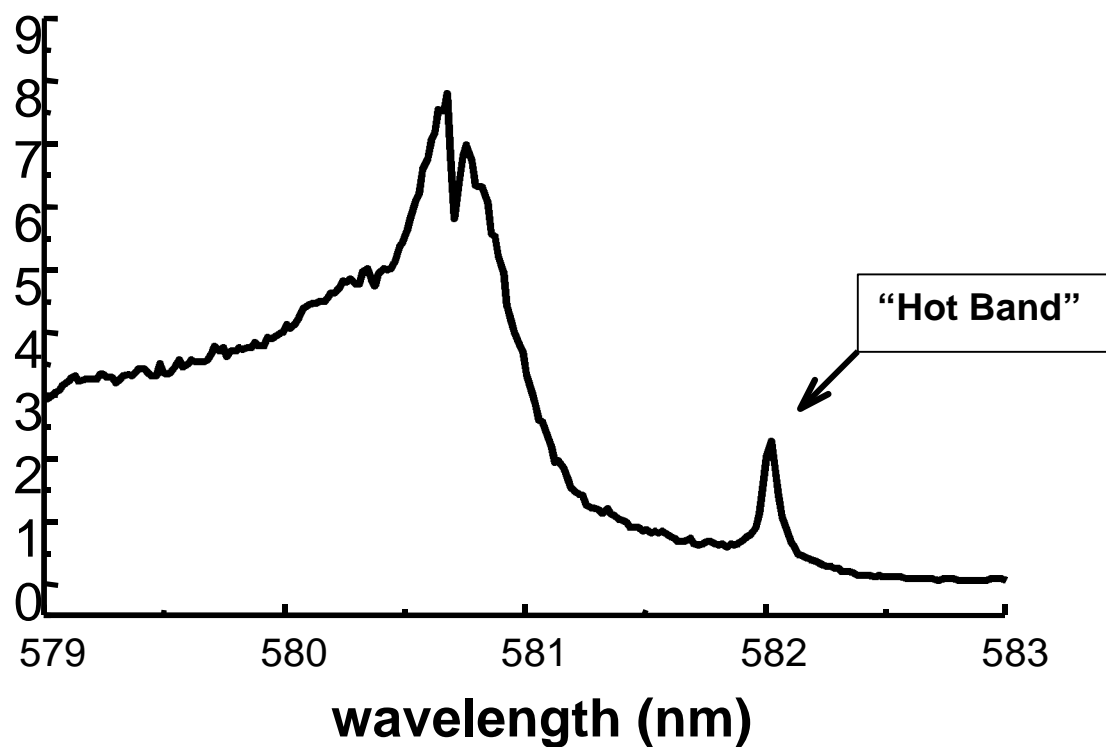


Figure 13. Fluorescence excitation spectrum of Eu₂O₃ (cubic-phase, micron-sized crystals). Fluorescence measured at $\lambda_{em} = 612\text{-nm}$.

The “hot band” corresponds to the ${}^7F_1 \rightarrow {}^5D_0$ transition.

level are referred to as “hot bands” because the 7F_1 level is populated by heat. The size of the “hot bands” is directly proportional to the amount of heat in the system. An attempt was made to heat the system by holding the excitation wavelength on the “hot band” at 582 nm. If heat was accumulated between laser pulses the intensity of the “hot band” should increase over time. After 20 minutes 12,000 laser pulses had excited the Eu_2O_3 sample but the intensity of the “hot band” had not changed. This proved that any heat produced was removed by the refrigeration system before the next excitation pulse.

From the arguments presented above, localized heating seems an extremely unlikely explanation for the saturation dips.

3.7 UP-CONVERSION BY ENERGY TRANSFER

Up-conversion is a special type of cross-relaxation involving two excited ions. Conventionally cross-relaxation involves an excited ion and an ion in the ground state. However if the excited-state density is high, the probability that two excited ions will be in close proximity increases and it is possible that cross-relaxation will occur between two excited ions. The mechanism for up-conversion is presented in Figure 14. Usually two identical excited ions are de-excited, and one highly excited ion and one ground state ion are produced. In the case of Eu_2O_3 , the highly excited ion decays nonradiatively to the lowest excited state. As excitation density is increased, the process of up-conversion gives rise to a new decay channel in Eu_2O_3 . This explains the observed

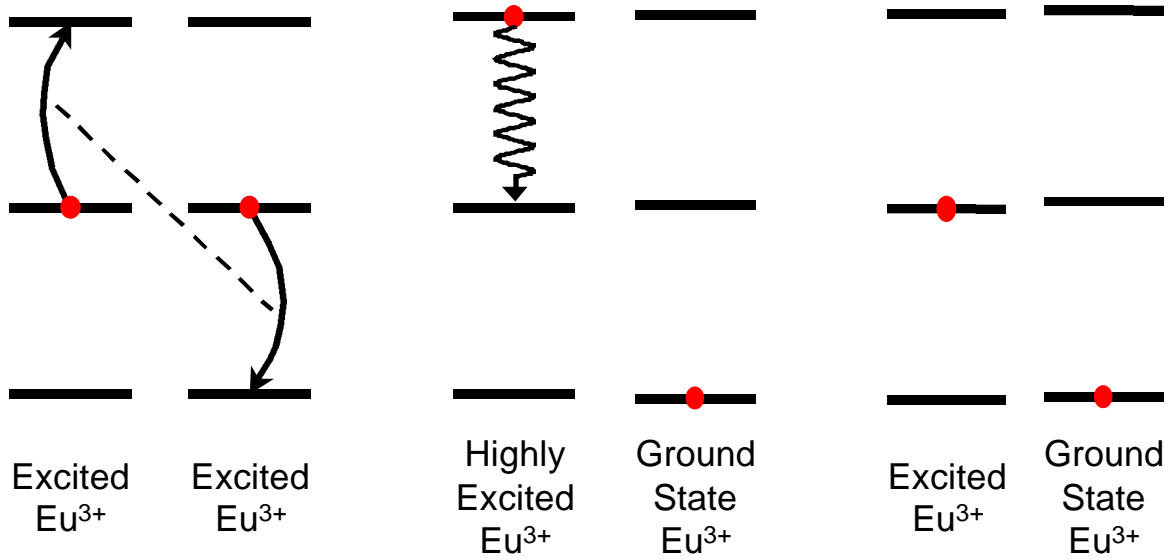


Figure 14. Upconversion by Energy Transfer in Eu_2O_3

intensity-dependent nonexponential decay. It also explains the saturation dips in the excitation spectra since up-conversion would cause a significant reduction in quantum efficiency at high-excited state densities achievable only at absorbance maxima.^[9]

The process of up-conversion by energy transfer has been documented for many concentrated lanthanide systems. Two examples, which provide good comparisons to Eu_2O_3 , are the concentrated Terbium compounds TbPO_4 and TbF_3 . In TbPO_4 a non-exponential decay of the fluorescent radiation was ascribed to up-conversion by energy transfer. The rate of up-conversion gn , was proportional to the excited state density n , with up-conversion coefficient $g = 5 \times 10^{-15} \text{ cm}^3\text{sec}^{-1}$.^[1] The determination that the non-exponential decay was due to up-conversion was made easier by the observation of anti-Stokes luminescence. An energy level diagram depicting the process of up-conversion in TbPO_4 is presented in Figure 15. A tunable dye laser was used to excite the Tb^{3+} ion's $^5\text{D}_3$ energy level at $20,440 \text{ cm}^{-1}$. The process of up-conversion combined the energy of two excited Tb^{3+} ions producing one highly excited ion with energy of $40,840 \text{ cm}^{-1}$. The highly excited ion then decays nonradiatively between the other $4f^8$ levels until reaching the $^5\text{D}_3$ energy level. Emission from the $^5\text{D}_3$ level results in anti-Stokes luminescence. Unlike Eu_2O_3 , the presence of anti-Stokes radiation from TbPO_4 allows for easy confirmation of up-conversion. The influence up-conversion has on luminescence decay is also more obvious for TbPO_4 (refer to Figure 16). Under low excitation density the luminescence decays exponentially. However under conditions of high

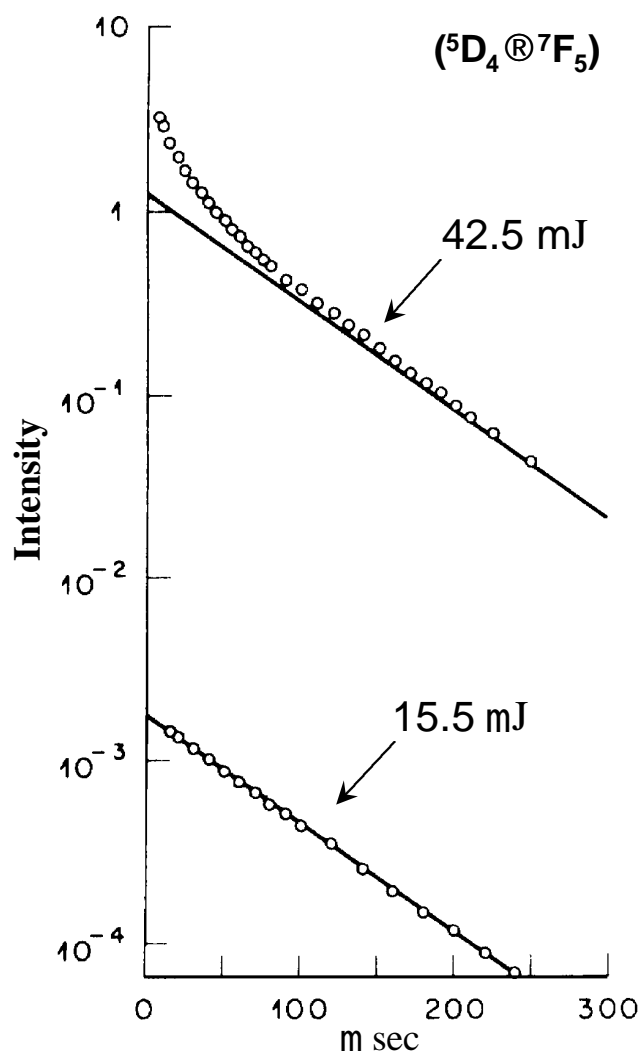


Figure 16. Dependence of 5D_4 decay time on excitation density for $TbPO_4$.

Reprinted from Solid State Communications, Volume 18, Diggle, P.C., Gehring, K. A., Macfarlane, R. M., "Exciton-exciton Annihilation in $TbPO_4$ ", Pages No. 392, Copyright 1976, with permission from Elsevier Science.

excitation density up-conversion provides an additional decay pathway and the luminescence decay becomes nonexponential.

Another compound in which up-conversion by energy transfer occurs is TbF_3 . As in TbPO_4 , up-conversion is easily confirmed by the presence of anti-Stokes radiation. As well as being an additional example of up-conversion in a concentrated rare earth system, TbF_3 is particularly relevant, because like Eu_2O_3 , dips appear in the center of each excitation peak.^[10] Examples of TbF_3 excitation spectra taken at high and low excitation densities are presented in Figure 17. Examples of Eu_2O_3 excitation spectra taken at similar conditions using a fused crystal sample are presented for comparison in Figure 18. The excitation density achievable in the study on TbF_3 was high enough that the dips in the excitation spectra actually reaches the noise level of the photomultiplier.^[10] This level of excitation density was not achievable in my study of Eu_2O_3 due to the power limitations of my excitation source. Fortunately the excitation intensity required to produce up-conversion in Eu_2O_3 is much less than that of TbF_3 , because the oscillator strength for transitions in Eu_2O_3 is nearly 1000 times larger than in TbF_3 .^[9]

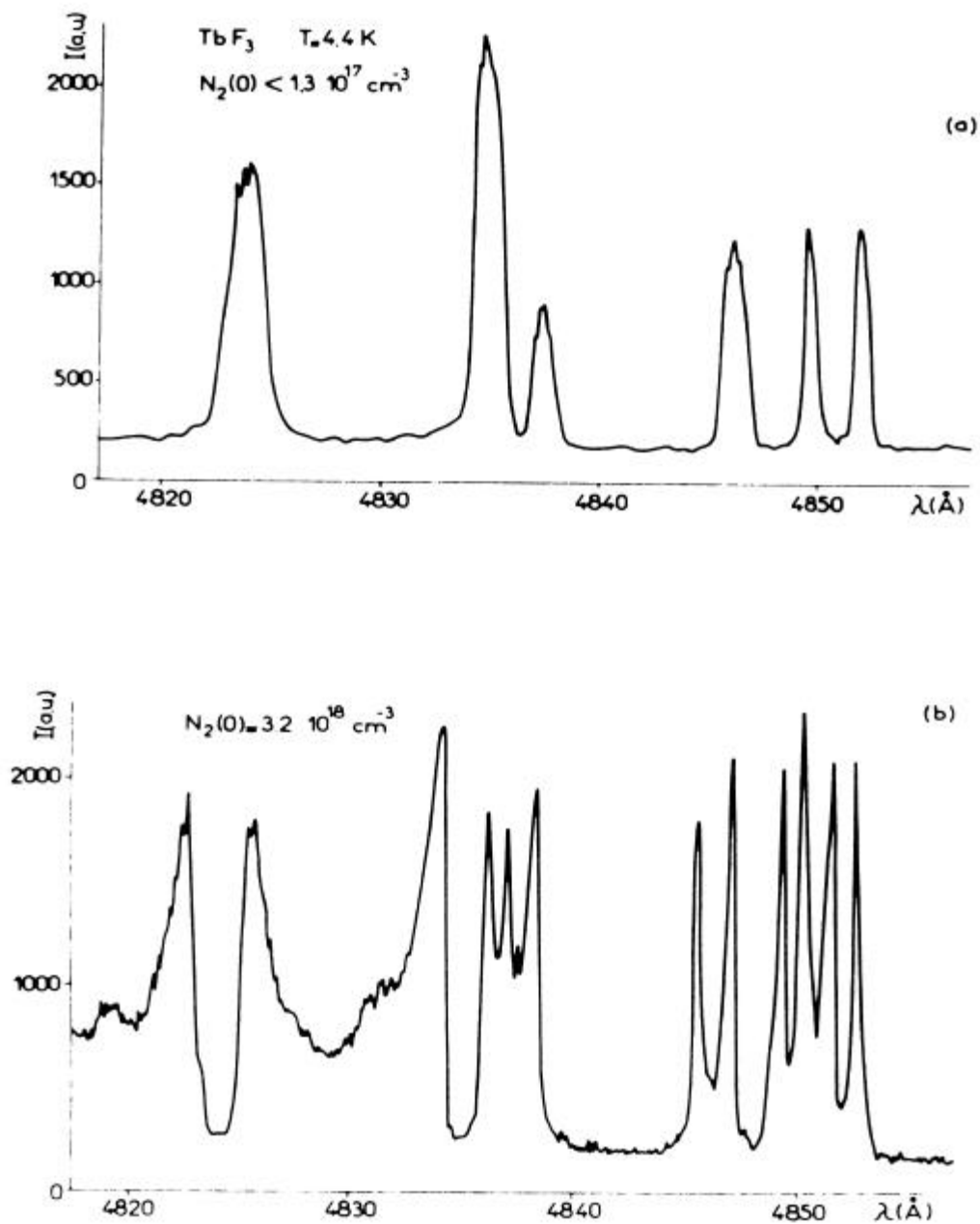
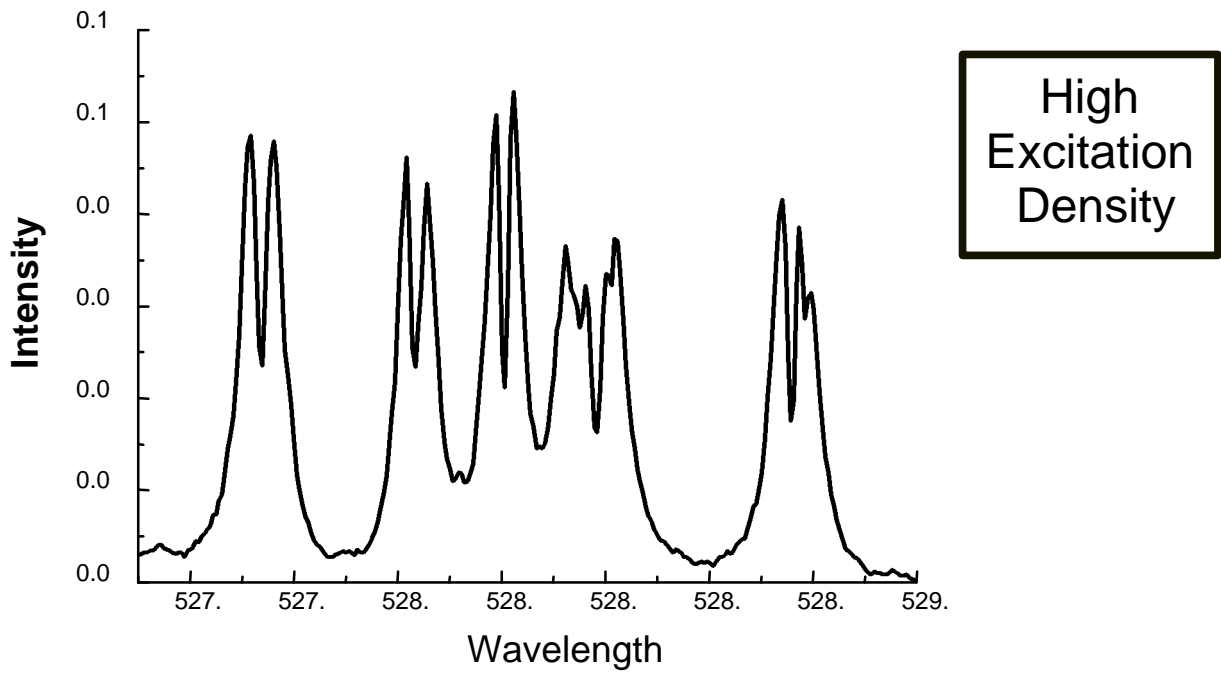
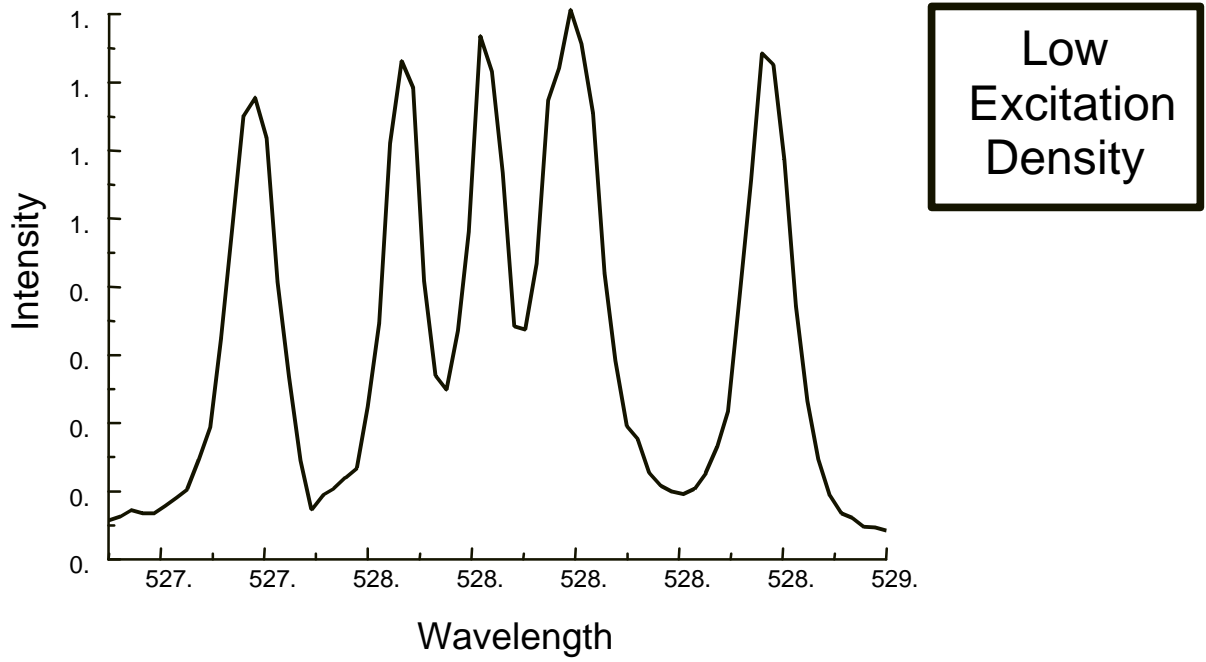


Figure 17. Excitation spectra of the blue fluorescence line of TbF₃ located at 486.3 nm (20,560cm⁻¹)
(a) Low excitation density
(b) High excitation density

Reprinted from Physical Review B, Volume 28, Issue 7, Joubert, M. F., Jacquier, B., Moncorge, "Exciton-exciton annihilation and saturation effect in TbF₃", Page No. 3727, Copyright 1983, with permission from Dr. Marie-France Joubert.



**Figure 18. Upconversion in Eu_2O_3
(monoclinic-phase, large fused crystal)**

3.8 LUMINESCENCE DECAY TRANSIENTS

The luminescence decay of Eu_2O_3 is always nonexponential regardless of excitation density. The decay pattern of Eu_2O_3 is characteristic of 3-dimensional diffusion-limited energy migration (for additional information refer to the Appendix). It is initially non-exponential and becomes exponential after long times. This makes it difficult to quantify the excitation density at which up-conversion begins to influence luminescence decay. However examination of luminescence decay at various excitation densities does support the up-conversion theory (refer to Figure 19). The data presented in Figure 19 shows normalized luminescence decay curves taken at various excitation energies. It is clear that the lifetime shortens and becomes increasingly nonlinear as excitation energies are increased. This is consistent with the additional density-dependent decay pathway that up-conversion would provide.

Evidence of excitation-density-dependent decay is most easily presented through the use of luminescence decay measurements. A series of luminescence transients were collected for a number of different Eu_2O_3 samples. Each of the decay transients was fit with a mathematical equation to allow the data to be presented concisely in tables. In most cases the decay transients were fit with the dual exponential decay function:

$$y = y_0 + A_1 \cdot \exp(-(x-x_0)/t_1) + A_2 \cdot \exp(-(x-x_0)/t_2)$$

In cases of very high excitation density the decay is so fast that a sum of three

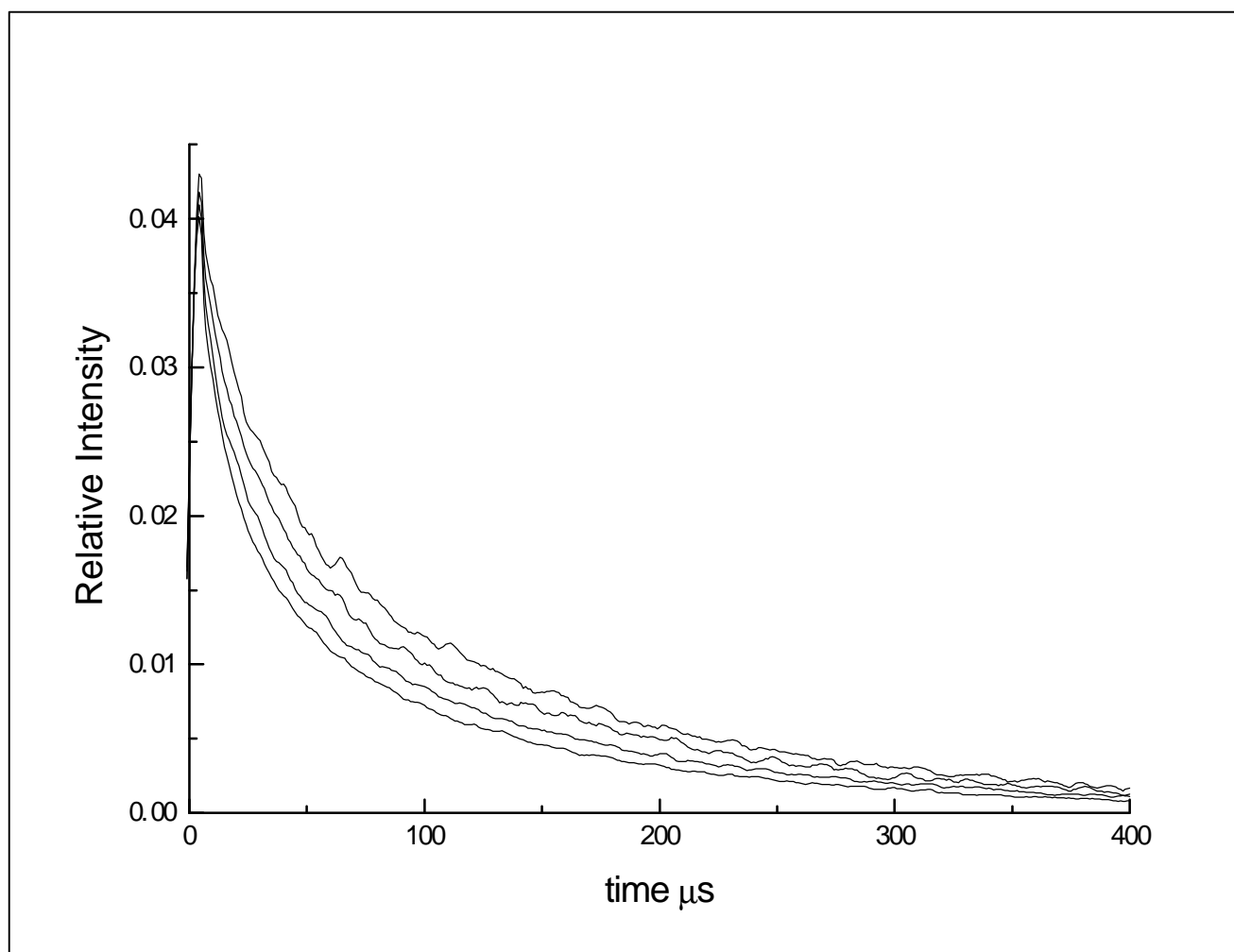


Figure 19. Normalized luminescence decay curves of Eu₂O₃ (cubic-phase) measured at various laser intensities.

exponential decay functions must be used:

$$y = y_0 + A_1 \exp(-(x-x_0)/t_1) + A_2 \exp(-(x-x_0)/t_2) + A_3 \exp(-(x-x_0)/t_3)$$

The first set of transients (refer to Table 2) is of cubic-phase Eu_2O_3 powder. The crystals are micron-sized. The wavelengths 525.97, 526.09, 527.36, and 527.90 nm correspond to excitation at the absorption maxima of ${}^7\text{F}_0 \rightarrow {}^5\text{D}_1$ transitions. The wavelengths 526.11, 527.80, and 527.90 nm correspond to excitation slightly off of absorption maxima for comparison. Luminescence decay corresponding to the ${}^5\text{D}_0 \rightarrow {}^7\text{F}_2$ transition was then recorded at 611.2 nm in all cases. The excitation density is proportional to the laser excitation energy listed in mJoules. As the excitation density is increased the luminescence decay becomes faster due to the increased contribution of nonlinear quenching, and this can be seen in the decrease in the time constants t_1 , t_2 , and t_3 . The increase in the rate of luminescence decay is larger when exciting at peak maxima compared to off peak maxima, because the higher the excited-state density the larger the contribution of nonlinear quenching. This explains why the saturation dip can only be produced at absorption maxima.

A similar trend can be seen when exciting into the ${}^7\text{F}_0 \rightarrow {}^5\text{D}_0$ transition of cubic phase Eu_2O_3 powder (refer to Table 3). In this case the absorption maximum occurs at 580.7 nm.

excited	Laser Energy (J)	A1	%A1	t1	A2	%A2	t2	A3	%A3	t3	A1+A2+A3
525.97	48	0.000	0%	0	0.113	68%	12.5	0.054	32%	69.2	0.167
525.97	78	0.128	52%	8.5	0.093	37%	33.8	0.028	11%	118.1	0.249
525.97	117	0.195	59%	8.8	0.106	32%	36.6	0.029	9%	126.9	0.330
525.97	156	0.211	49%	6.1	0.158	37%	22.3	0.059	14%	83.7	0.429
526.09	48	0.000	0%	0	0.128	68%	11.5	0.061	32%	66.9	0.189
526.09	78	0.148	54%	8.3	0.096	35%	31.8	0.033	12%	111.3	0.277
526.09	123	0.206	47%	5.5	0.163	37%	20.3	0.067	15%	77.6	0.436
526.09	156	0.255	53%	6.3	0.165	34%	22.9	0.061	13%	84.7	0.482
526.11	48	0.000	0%	0	0.084	68%	17.6	0.040	32%	85.6	0.124
526.11	78	0.121	57%	10.8	0.073	34%	45.6	0.018	8%	145.8	0.211
526.11	123	0.161	55%	8.9	0.100	34%	35.9	0.031	11%	124.5	0.292
526.11	165	0.195	51%	7.4	0.135	35%	26.5	0.053	14%	93.1	0.383
527.36	48	0.000	0%	0	0.220	72%	8.3	0.086	28%	54.1	0.306
527.36	75	0.143	29%	2.4	0.254	52%	10.6	0.094	19%	54.7	0.491
527.36	117	0.263	40%	3	0.304	46%	11.5	0.099	15%	57.7	0.666
527.36	171	0.289	33%	2	0.458	52%	9	0.135	15%	48.9	0.882
527.36	240	0.463	46%	3.3	0.413	41%	11.9	0.121	12%	56.2	0.997
527.8	54	0.000	0%	0	0.119	67%	13.7	0.059	33%	74.3	0.178
527.8	75	0.124	49%	8.1	0.099	39%	31.5	0.032	12%	115.3	0.255
527.8	132	0.198	48%	5.9	0.151	37%	20.6	0.064	16%	79.1	0.413
527.8	180	0.280	54%	5.8	0.174	33%	21.5	0.067	13%	82	0.521
527.8	255	0.377	54%	5.2	0.235	34%	18.7	0.086	12%	74.3	0.698
527.87	54	0.000	0%	0	0.352	70%	4.6	0.149	30%	32.4	0.500
527.87	81	0.212	32%	1.8	0.343	52%	8.5	0.104	16%	48.8	0.659
527.87	135	0.299	32%	1.3	0.490	53%	7.1	0.134	15%	42.5	0.923
527.87	189	0.465	33%	0.4	0.734	51%	4.7	0.227	16%	27.7	1.426
527.87	258	0.606	35%	0.4	0.893	51%	5.2	0.236	14%	28.3	1.735
527.9	54	0.000	0%	0	0.172	69%	9.5	0.076	31%	61.4	0.249
527.9	81	0.138	38%	4.1	0.162	44%	15.5	0.067	18%	67.9	0.367
527.9	138	0.185	34%	2.9	0.258	48%	11.8	0.095	18%	59.6	0.538
527.9	186	0.248	38%	3.2	0.299	46%	12.1	0.104	16%	59	0.652
527.9	261	0.335	42%	3.2	0.352	44%	12.8	0.108	14%	59.1	0.795

**Table 1. Decay constants calculated for Eu₂O₃ powder (cubic-phase, micron-sized particles) using a sum of three exponential decay functions:
 $y = y_0 + A1 \cdot \exp(-(x-x_0)/t1) + A2 \cdot \exp(-(x-x_0)/t2) + A3 \cdot \exp(-(x-x_0)/t3)$.
The sample was excited into the ⁵D₁ energy level.**

excited	Laser Energy (J)	A1	%A1	t1	A2	%A2	t2	A1+A2
568.5	66	0.034	57%	36.1	0.025	43%	139.3	0.059
568.5	99	0.066	60%	25.9	0.044	40%	113.1	0.110
568.5	153	0.099	61%	21.5	0.063	39%	101.8	0.162
568.5	195	0.134	64%	19.5	0.075	36%	94.6	0.209
570.4	66	0.019	51%	33.2	0.018	49%	120.6	0.037
570.4	105	0.052	54%	41.9	0.045	46%	134	0.096
570.4	165	0.026	55%	35.6	0.021	45%	125	0.047
570.4	216	0.033	59%	35.8	0.023	41%	124.6	0.056
580.5	105	0.039	60%	34.5	0.026	40%	119.4	0.065
580.5	189	0.081	62%	23.7	0.049	38%	101.1	0.130
580.5	255	0.107	61%	17.9	0.067	39%	87.2	0.174
580.6	48	0.041	61%	31	0.027	39%	115.4	0.068
580.6	99	0.108	64%	17.2	0.061	36%	85.9	0.170
580.6	189	0.204	68%	13.1	0.095	32%	75.1	0.300
580.6	240	0.250	66%	10.9	0.131	34%	57.5	0.381
580.7	48	0.188	70%	8.6	0.079	30%	59.9	0.267
580.7	99	0.356	70%	5.9	0.154	30%	41.2	0.510
580.7	186	0.591	66%	3.8	0.300	34%	24.8	0.891
580.7	240	0.684	67%	3.7	0.330	33%	24.1	1.014
580.8	48	0.031	57%	25.6	0.023	43%	110.2	0.054
580.8	99	0.065	61%	19.1	0.041	39%	92.2	0.107
580.8	186	0.123	65%	15	0.067	35%	79.2	0.190
580.8	243	0.152	67%	14.6	0.075	33%	77.2	0.227
580.9	45	0.034	57%	52	0.025	43%	143.7	0.059
580.9	99	0.072	59%	37.3	0.050	41%	124.2	0.122
580.9	180	0.040	62%	32.1	0.025	38%	116.8	0.065
580.9	243	0.057	63%	26.1	0.033	37%	105.5	0.091

Table 2. Decay constants calculated for Eu₂O₃ powder (cubic-phase, micron-sized particles) using a sum of two exponential decay functions:

$$y = y_0 + A_1 \cdot \exp(-(x-x_0)/t_1) + A_2 \cdot \exp(-(x-x_0)/t_2).$$

Excitation was to the ⁵D₀ energy level. The maximum absorbance for the ⁷F₀ → ⁵D₀ transition occurs at 580.7 nm, and excitation slightly off maximum (580.5, 580.6, 580.8, and 580.9 nm) is presented for comparison. Excitation at 568.5 nm and 570.4 nm include energy contributions from lattice vibrations.

Luminescence decay measurements of Eu_2O_3 nanocrystals are presents as a function of excitation density (refer to Tables 4&5). The average diameter of the nanocrystals in Tables 4 and 5 are estimated as 10 nm and 20 nm respectively, however an exact size distribution was not determined. The excitation maxima corresponds to slightly different wavelengths in this case because the nanocrystals can only be prepared in the monoclinic phase. The same excitation-density-dependent decay trend, however, that was seen in the micron-sized particles was also seen in the nanocrystals. The effects nonlinear quenching does not appear to be size dependent.

The most profound increases in luminescence decay rate as a function of excitation density was seen in the large fused Eu_2O_3 crystal (refer to Table 6). Higher excited-state densities were producible with the large crystal because the exciting laser beam can be more sharply focused on the sample surface, unlike with powdered samples where laser scattering is unavoidable.

λ excited	Laser Energy (J)	A1	%A1	t1 (s)	A2	%A2	t2 (s)	A1+A2
526.75	30	0.050	61%	2.8	0.032	39%	10.9	0.082
526.75	150	0.097	71%	3.3	0.040	29%	13.1	0.137
526.75	225	0.115	61%	2.2	0.075	39%	10.3	0.189
527.73	60	0.034	71%	4.6	0.014	29%	16.7	0.048
527.73	159	0.059	70%	3.9	0.025	30%	16.6	0.084
527.73	243	0.071	70%	4.0	0.030	30%	17.5	0.101
528.34	63	0.044	75%	4.8	0.015	25%	17.9	0.059
528.34	162	0.080	75%	4.3	0.027	25%	18.3	0.107
528.34	243	0.092	74%	4.4	0.032	26%	19.2	0.124
528.73	66	0.044	74%	4.6	0.015	26%	18.7	0.060
528.73	165	0.077	71%	3.9	0.031	29%	17.7	0.108
528.73	246	0.092	74%	4.4	0.032	26%	20.0	0.124
535.4	48	0.008	44%	3.1	0.011	56%	10.2	0.019
535.4	108	0.025	68%	4.2	0.012	32%	12.7	0.037
535.4	156	0.031	67%	4.3	0.015	33%	12.3	0.046
578.45*	66	0.043	75%	6.3	0.014	25%	24.6	0.057
578.45*	159	0.095	75%	5.1	0.032	25%	22.6	0.127
578.45*	228	0.123	71%	4.2	0.049	29%	19.4	0.173
578.54	66	0.089	76%	4.3	0.029	24%	17.8	0.118
578.54	156	0.158	68%	2.9	0.075	32%	13.6	0.233
578.54	225	0.203	71%	2.9	0.085	29%	14.0	0.288
578.6*	66	0.053	80%	5.8	0.013	20%	21.1	0.066
578.6*	153	0.103	75%	4.3	0.034	25%	17.0	0.136
578.6*	225	0.140	71%	3.2	0.058	29%	13.8	0.198
578.65*	66	0.025	67%	5.2	0.012	33%	16.4	0.037
578.65*	153	0.051	67%	4.1	0.026	33%	15.8	0.077
578.65*	225	0.079	73%	4.3	0.029	27%	16.9	0.108

**Table 3. Decay constants calculated for Eu_2O_3 powder (monoclinic-phase, ~10 nanometer-sized particles) using a sum of two exponential decay functions:
 $y = y_0 + A1 \cdot \exp(-(x-x_0)/t1) + A2 \cdot \exp(-(x-x_0)/t2)$.
Excitation at 526.75, 527.73, and 528.34 nm corresponds to the ${}^7\text{F}_0 \rightarrow {}^5\text{D}_1$ transition. Excitation at 535.4 nm includes energy contributions from lattice vibrations. Excitation at 578.54 nm corresponds to the absorbance maximum of the ${}^7\text{F}_0 \rightarrow {}^5\text{D}_0$ transition, and excitation at 578.45, 578.6, and 578.65 nm are slightly off maximum for comparison.**

λ excited	Laser Energy (J)	A1	%A1	t1 (s)	A2	%A2	t2 (s)	A1+A2
526.75	5.7	0.039	79%	10.3	0.010	21%	59.1	0.049
526.75	57	0.326	73%	4.7	0.118	27%	29.1	0.444
526.75	144	0.704	73%	3.6	0.260	27%	21.7	0.964
526.75	270	0.985	58%	1.9	0.707	42%	11.9	1.691
527.73	6.6	0.030	76%	9.3	0.010	24%	50.7	0.040
527.73	66	0.316	73%	5.1	0.116	27%	30.9	0.433
527.73	168	0.652	73%	4.1	0.240	27%	24.0	0.891
527.73	285	0.984	67%	3.1	0.475	33%	16.4	1.459
528.34	7.5	0.042	79%	9.3	0.011	21%	57.0	0.053
528.34	75	0.449	75%	4.5	0.152	25%	27.6	0.602
528.34	180	0.879	77%	3.8	0.266	23%	23.6	1.144
528.34	285	0.520	65%	1.6	0.279	35%	12.4	0.798
528.73	7.8	0.055	79%	8.4	0.014	21%	50.2	0.070
528.73	78	0.476	74%	3.6	0.166	26%	23.9	0.641
528.73	180	0.847	74%	3.0	0.298	26%	19.7	1.145
528.73	297	0.507	65%	1.2	0.274	35%	11.0	0.781
535.4	5.4	0.013	71%	7.3	0.005	29%	38.3	0.018
535.4	54	0.116	71%	5.9	0.048	29%	35.3	0.164
535.4	105	0.212	73%	5.0	0.079	27%	31.6	0.291
535.4	165	0.112	71%	4.0	0.046	29%	25.7	0.158
578.45*	5.4	0.012	82%	12.2	0.003	18%	77.4	0.015
578.45*	54	0.139	71%	7.2	0.055	29%	42.3	0.194
578.45*	141	0.343	74%	6.1	0.120	26%	36.6	0.463
578.45*	240	0.205	73%	5.2	0.075	27%	33.1	0.280
578.54	5.4	0.025	81%	14.3	0.006	19%	80.6	0.031
578.54	54	0.296	74%	5.9	0.102	26%	34.2	0.398
578.54	141	0.663	75%	4.7	0.225	25%	26.9	0.888
578.54	240	0.351	71%	1.7	0.143	29%	11.1	0.494
578.6*	5.4	0.018	77%	11.1	0.005	23%	58.9	0.024
578.6*	54	0.226	74%	6.0	0.078	26%	35.2	0.304
578.6*	141	0.587	75%	4.5	0.199	25%	27.1	0.786
578.6*	240	0.377	67%	2.8	0.186	33%	17.7	0.563
578.65*	5.4	0.013	81%	12.2	0.003	19%	68.2	0.017
578.65*	54	0.141	73%	6.7	0.053	27%	39.1	0.194
578.65*	141	0.339	73%	5.0	0.127	27%	30.3	0.465
578.65*	240	0.200	73%	4.5	0.076	27%	28.4	0.276

Table 4. Decay constants calculated for Eu₂O₃ powder (monoclinic-phase, ~20 nanometer-sized particles). Excitation at 526.75, 527.73, and 528.34 nm corresponds to the ⁷F₀→⁵D₁ transition. Excitation at 535.4 nm includes energy contributions from lattice vibrations. Excitation at 578.54 nm corresponds to the absorbance maximum of the ⁷F₀→⁵D₀ transition, and excitation at 578.45, 578.6, and 578.65 nm are slightly off maximum for comparison.

λ excited	Laser Energy (J)	A1	%A1	t1 (s)	A2	%A2	t2 (s)	A1+A2
526.75	4.2	0.046	68%	24.2	0.022	32%	136.5	0.068
526.75	42	0.038	68%	20.0	0.018	32%	132.3	0.057
526.75	123	0.110	67%	13.1	0.054	33%	106.9	0.164
526.75	246	0.165	67%	12.5	0.080	33%	102.3	0.245
527.73	5.1	0.084	72%	17.8	0.033	28%	123.3	0.117
527.73	51	0.055	68%	12.4	0.026	32%	110.4	0.081
527.73	138	0.124	68%	9.5	0.059	32%	97.1	0.183
527.73	264	0.172	67%	9.4	0.084	33%	92.3	0.256
528.34	5.4	0.057	60%	18.5	0.038	40%	128.4	0.095
528.34	54	0.053	63%	17.5	0.031	37%	122.5	0.084
528.34	150	0.118	64%	15.8	0.067	36%	111.7	0.185
528.34	282	0.160	64%	16.2	0.088	36%	110.3	0.248
528.73	5.7	0.075	75%	11.9	0.025	25%	121.0	0.100
528.73	57	0.034	66%	9.3	0.018	34%	113.7	0.052
528.73	126	0.071	71%	9.7	0.029	29%	89.2	0.101
528.73	282	0.115	65%	8.1	0.061	35%	105.2	0.176
535.4	4.8	No Signal						
535.4	48	0.003	42%	10.5	0.004	58%	161.7	0.007
535.4	108	0.005	37%	19.8	0.009	63%	169.0	0.014
535.4	192	0.009	39%	13.6	0.014	61%	146.4	0.022
578.45*	4.8	0.018	40%	35.4	0.028	60%	165.2	0.046
578.45*	48	0.020	48%	30.9	0.021	52%	157.0	0.041
578.45*	123	0.049	53%	22.8	0.044	47%	143.5	0.094
578.45*	246	0.075	55%	22.7	0.060	45%	138.6	0.135
578.54	4.8	0.024	49%	27.4	0.025	51%	152.0	0.049
578.54	48	0.023	55%	24.4	0.019	45%	148.6	0.041
578.54	123	0.058	57%	18.8	0.043	43%	131.5	0.102
578.54	246	0.100	60%	16.2	0.067	40%	118.1	0.167
578.6*	4.8	0.007	36%	28.6	0.013	64%	177.4	0.020
578.6*	48	0.005	31%	23.0	0.012	69%	164.6	0.017
578.6*	120	0.061	40%	17.4	0.091	60%	148.0	0.152
578.6*	240	0.041	50%	13.6	0.041	50%	141.3	0.082
578.65*	4.8	0.003	31%	44.3	0.006	69%	197.6	0.009
578.65*	48	0.003	28%	28.9	0.007	72%	190.5	0.010
578.65*	120	0.026	29%	33.2	0.062	71%	171.8	0.088
578.65*	240	0.014	31%	26.2	0.032	69%	163.1	0.046

Table 5. Decay constants for Eu_2O_3 large fused crystal (monoclinic-phase) Excitation at 526.75, 527.73, and 528.34 nm corresponds to the ${}^7\text{F}_0 \rightarrow {}^5\text{D}_1$ transition. Excitation at 535.4 nm includes energy contributions from lattice vibrations. Excitation at 578.54 nm corresponds to the absorbance maximum of the ${}^7\text{F}_0 \rightarrow {}^5\text{D}_0$ transition, and excitation at 578.45, 578.6, and 578.65 nm are slightly off maximum for comparison.

Chapter 3 References

- [1] P. C. Diggle, K. A. Gehring, R. M. Macfarlane, *Solid State Communications* **1976**, *18*, 391.
- [2] M. C. Downer, in *Laser Spectroscopy of Solids II, Vol. 65* (Ed.: W. M. Yen), Springer-Verlag, Berlin, **1989**.
- [3] F. E. Auzel, in *RARE EARTHS SPECTROSCOPY* (Eds.: B. Jezowska-Trzebiatowska, J. Legendziewicz, W. Streck), World Scientific, Wroclaw, **1984**, pp. 502.
- [4] D. B. M. Klaassen, T. G. M. van Rijn, A. T. Vink, *J. Electrochem. Soc.* **1989**, *136*, 2732.
- [5] R. B. J. Hunt, R. G. Pappalardo, *Journal of Luminescence* **1985**, *34*, 133.
- [6] J. Rai, C. M. Bowden, *Physical Review A* **1992**, *46*, 1522.
- [7] M. Yin, J. C. Krupa, *Chemical Physics Letters* **1999**, *314*, 27.
- [8] M. Buijs, J. I. Vree, G. Blasse, *Chemical Physics Letters* **1987**.
- [9] R. L. Cone, R. S. Meltzer, in *Spectroscopy of Solids Containing Rare Earth Ions* (Eds.: A. A. Kaplyanskii, R. M. MacFarlane), Elsevier Science Publishers, North-Holland, **1987**, pp. 481.
- [10] M. F. Joubert, B. Jacquier, Moncorge, *Phys. Rev. B* **1983**, *28*, 3725.